THE JOURNAL OF PHYSICAL CHEMISTRY A

© Copyright 2008 by the American Chemical Society VOLUME 112, NUMBER 25, JUNE 26, 2008

ARTICLES

Fluorescence Spectroscopy and Amplified Spontaneous Emission (ASE) of Phenylimidazoles: Predicted Vibronic Coupling Along the Excited-State Intramolecular Proton Transfer in 2-(2′-Hydroxyphenyl)imidazoles

Juan Carlos del Valle,*,† R. M. Claramunt,‡ and J. Catalán*,†

Department of Química Física Aplicada, Universidad Autónoma de Madrid, Cantoblanco, C-2-203, E-28049 Madrid, Spain and Department of Química Orgánica y Biología, Facultad de Ciencias, UNED, Senda del Rey 9, E-28040 Madrid, Spain

Received: July 5, 2007; Revised Manuscript Received: April 14, 2008

Methylation at the 1N position of 2-phenylimidazole provides the shortest wavelength for a liquid-state laser dye reported to date; that is, the 1-methyl-2-phenylimidazole molecule in cyclohexane solution yields amplified spontaneous emission (ASE) with a peak wavelength at 314.5 nm and a constant laser gain value of 5 cm^{-1} from 310 to 317 nm. Methyl substitution in this case favors the appearance of laser action (owing to a torsion−vibrational mechanism) in cyclohexane as compared with the nonmethylated species which does not exhibit ASE in this solvent. The 2-(2′-hydroxyphenyl)imidazole molecules give rise to ASE with high gain values (ca. 9 cm^{-1}) at 450 and 466 nm. The mechanism of population inversion is understood in terms of a vibronic coupling between the hydroxyl stretching motion and the torsional vibration of the phenyl and imidazole rings. The proton-transfer spectroscopy of 2-(2′-hydroxyphenyl)imidazoles is studied in dioxane, cyclohexane, dimethyl sulfoxide, methanol, and water. The greater the acidity of the solvent the greater the disruption of the intramolecular hydrogen bond; solvent acidity is the main parameter which favors formation of the open-form species in the ground electronic state. Methyl substitution at the 1N position favors formation of the open species for 2-hydroxyphenylimidazoles in the ground electronic state, which decreases their own capacity to undergo ASE. Low-temperature absorption spectroscopy confirms aggregation processes for 2-(2′-hydroxyphenyl)imidazoles in solution. In accordance with X-ray analyses in the solid phase, these molecules form associations through intermolecular chains of the type N—H···O or O—H···N.

I. Introduction

Laser spectroscopy has dealt with the research of the mechanisms responsible for the laser action monitored in many molecular,[1–3] ion,[2–5] and atomic systems[2,6] with the aid of light absorption and emission techniques with special emphasis in the UV region in which obtaining molecular−dye systems with high laser gain has taken much effort.

Among the molecular−dye laser systems, those concerned with the proton-transfer mechanism in the excited state guarantee population inversion,[7] thus presenting high laser gains. The first proton-transfer laser was proposed in 1983 based on the 3-hydroxyflavone molecular structure;[7,8] this molecule presents

* Corresponding authors. Phone: +91-4974263. Fax: +91-4974785. E-mail: juan.valle@uam.es; rclaramunt@ccia.uned.es; Javier.catalan@uam.es.
† Universidad Autónoma de Madrid.
‡ UNED.

10.1021/jp7117604 CCC: $40.75 © 2008 American Chemical Society
Published on Web 05/30/2008

an excited-state *intramolecular*-proton-transfer (ESIPT) process which yields laser action. Other pioneer families of ESIPT lasers were reported in 1986, for instance, the salicylamide,[9] sodium salicylate,[10] and 2-(2-hydroxyphenyl) benzimidazole[10,11] molecular lasers with efficiencies up to 10%. However, all of them exhibit lasing action in the visible spectral region.

Another laser mechanism proposed to develop lasing action in the UV spectrum consisted of a torsion−conformational change undergone on photoexcitation of 2-phenylbenzimidazole and its derivatives.[12,13] The inter-ring torsion turns out to be essential to develop the lasing action, which also possesses large gain coefficient values. In any case, as previously published[7,12,13] the population-inversion requirement is supplied by a large or significant structural change on electronic excitation. For instance, if upon photoexcitation the structural change is not significant, the population inversion is not attained and the molecular system does not undergo laser or amplified spontaneous emission (ASE), as occurs for the fluorene molecule.[14]

Interestingly, the amplified spontaneous emission (ASE, lasing action) of a hydroxyl-substituted tetraphenylimidazole (i.e., acetic acid 2-{4-[2-(2-hydroxyphenyl)-4,5-diphenylimidazol-1-yl]phenyl}-ethylester)[15] has been recently reported from a large single crystal owing to an ESIPT mechanism.

We propose simple phenylimidazole structures, which reduce its heterocyclic size, to undergo laser emission with high gain values in the UV region, displaying a significant and sufficient structural change upon photoexcitation and a comprehensive molecular laser mechanism. The population-inversion mechanism involved in 2-(2′-hydroxyphenyl)imidazole (2HOPI) will be explored from a theoretical and experimental point of view. This mechanism consists of an excited-state proton-transfer process along with a vibronic coupling between the intramolecular hydroxy stretching and the inter-ring torsional vibration (vide infra). A methyl substitution has been undergone at the pyrrole nitrogen of 2-(2′-hydroxyphenyl)imidazole (1M2HOPI) in order to better visualize this vibronic coupling.

From an experimental point of view, nothing has been published on the photophysics of the 2HOPI and 1M2HOPI molecules. Nevertheless, experimental evidence was reported[16] on some derivatives of 2HOPI which exhibited large molar absorption coefficients ($\varepsilon_{max} \cong 20\,000$ M^{-1} cm^{-1}) in cyclohexane, thus featuring π,π^* transitions, for instance, 4,5-diphenyl-2-(2′-hydroxyphenyl)imidazole (DPHPI), 4,5-dimethyl-2-(2′-hydroxyphenyl)imidazole (DMeHPI), and methylphenyl-2-(2′-hydroxyphenyl)imidazole (MePHPI). It is also reported[16] that the shape and position of the first absorption bands change scarcely with solvent polarity, thus proving that the n,π^* states are shifted to higher energies, owing to the intramolecular hydrogen interaction with the nonbonding electrons of the pyridinic nitrogen. A planar ground-state conformation is predicted on the basis of the red shift found for the first absorption band for MePHPI as compared to that for DPHPI, from 304[17] to 325 nm, respectively.[16] The fluorescence of DMeHPI in cyclohexane, acetonitrile, and *p*-dioxane showed only one emission band (with respective quantum yields of 0.47, 0.48, and 0.55) largely shifted from the corresponding absorption spectrum (8320, 7762, and 7854 cm^{-1}, respectively), thus assigned to ESIPT emission.[16] The corresponding stimulated emission (obtained by using a resonant cavity)[16] pumped with an XeCl laser at 308 nm showed large gain values in acetonitrile and *p*-dioxane, 8.9% and 12.1%, respectively.

DMeHPI (at ca. 350 nm) and MePHPI presented an extra emission band in methanol and dimethylformamide also ascribed to the solvated open form.[16] In water at neutral pH, for instance, DMeHPI showed a chemical equilibrium between the open form and the keto form in the ground state.[18]

SCHEME 1: Closed-Form Molecular Structures for 2HOPI, 1M2HOPI, and 2MeOPI[a]

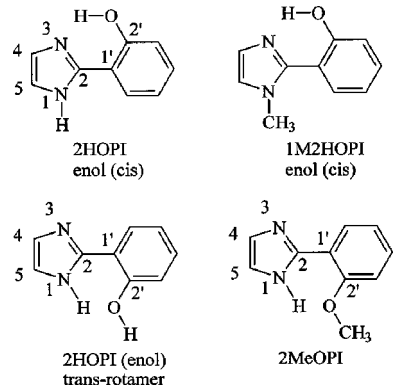

[a] The atom numbering is implemented.

The rotamerism and ESIPT processes for the S_1, T_1, and S_o states of the 2-(2′-hydroxyphenyl)imidazole (2HOPI) were investigated at the AM1 level using configurational interaction with single excitations (CIS)[19] and at the HF/CIS/D95** level.[20] These calculations have addressed both ESIPT and rotamerism, separate and uncoupled, processes.[19,20]

Basically, the same conclusions have been drawn in both of these studies.[19,20] (I) Rotamerism in 2HOPI in the ground and the first singlet π,π^* excited state indicates that the cis (enol form, closed form) and trans rotamers (another closed form) are interconvertible in the ground state but not in the first excited state. (II) The two tautomers keto−enol of 2HOPI become closer in energy compared to the ground state (ca. 27 kcal/mol energy difference), thus giving rise to an exothermic process in the T_1 state and S_1 state. (III) The energy barrier for the proton-transfer process decreases upon excitation to the T_1 and S_1 states. The keto form is less destabilized than the enol form also for the ^{1}n,π^* (S_2 state) excitation.[20]

However, it is well known that the HF and CIS/HF treatments overestimate the hydrogen-bond interactions (as well as the AM1 method), and they usually predict too high proton-transfer barriers,[21–23] owing to the neglect of electronic correlation (i.e., $\Delta E_{enol\text{-}keto}$ for 2HOPI in S_o, $S_1 - \pi,\pi^*$, $S_2 -$ n,π^*, and $T_1 - \pi,\pi^*$ results in 17.6, 9.3, 15.4, and 17.7 kcal/mol, respectively).[20]

The theoretical framework introduced in the following study on 2HOPI and its 1N-methylated derivative is intended to combine both processes, the inter-ring torsion and ESIPT, and shed light on the experimental evidence. As described in the Theoretical and Experimental Methods section, DFT methodology and the TD/CIS approach have been utilized for the sake of taking into account a greater contribution for the electronic correlation.

II. Theoretical and Experimental Methods

A. Absorption Spectroscopy. Absorption measurements were made for the various phenylimidazoles (Scheme 1) in solution at 298 K in the solvents given in the text and figure legends. The absorption spectra were recorded with the aid of a Shimadzu UV-2100 spectrophotometer.

Absorption from room temperature (RT) to 110 K (slow freezing) was recorded with the aid of a Cary 5 spectrometer (Varian) and a cryostat Oxford Optistat DN, which uses liquid nitrogen to control temperature. The solvents were of spectrometric quality and checked for fluorescence impurities.

B. Emission Spectroscopy. Emission spectra were obtained with the aid of an AB2 Aminco-Bowman Series 2 luminescence spectrometer. All spectra were recorded at 298 and 77 K. The low-temperature (quick freezing) fluorescence in methylcyclohexane and cyclohexane was recorded using a liquid nitrogen Dewar, which was built in a sample chamber purged with pure and dry N_2 gas. Fluorescence spectra were corrected for instrumental sensitivity when plotted together with the corresponding ASE spectra.

Emission spectra from RT to 113 K (slow freezing) were recorded with the aid of AB2 Aminco-Bowman Series 2 luminescence spectrometer and a cryostat Oxford Optistat DN, which uses liquid nitrogen to control temperature.

Fluorescence quantum yields were measured at 298 K on freshly prepared samples with absorbances at the excitation wavelength of ca. 0.1. The fluorescence standard 2-aminopyridine ($\Phi_f = 0.66$)[24] in 0.1 N H_2SO_4 was used for the measurements, which were corrected by taking into account the refractive index of the solvent.

Fluorescence lifetimes were determined with a phase and modulation spectrofluorimeter (SLM 48000S) at frequencies between 1 and 250 MHz.[25] Decisions on the suitability of the lifetimes rested on examination of the residual deviations with frequency and the reduced χ^2 values, which were close to unity. The detection limit of our instrument is ca. 30 ps.

C. Amplified Spontaneous Emission (ASE) Spectroscopy. The ASE laser spike measurements[12,26,27] were made by primary excitation with a Nd:YAG laser (Spectra-Physics model DCR-3G) using the fourth harmonic (266 nm) for 1-methyl-2-phenylimidazole (1M2PI), 2-(2′-hydroxyphenyl)imidazole (2HOPI), 1-methyl-2-(2′-hydroxyphenyl)imidazole (1M2HOPI), and 2-(2′-methoxypheny)imidazole (2MeOPI). The output of the Nd:YAG laser was focused to a narrow line in the dye cell in a transverse geometry. A DL 251 laser dye cell of 0.8 cm optical length with oblique windows was used (NSG precision cells Inc.), thus preventing optical feedback. The dye solution was stirred to prevent secondary processes, such as, for example, local heating, from interfering with the experiments. The ASE signal was dispersed by a 300 lines/mm and 0.32 m polychromator (Instruments SA model HR320) detected by an optical multichannel analyzer (OMA) system consisting of an intensified silicon photodiode array (EG and G/PAR, model 1421) and analyzed by a system processor (EG and G/PAR, model 1461/1463). To reduce the noise, the detector was operated in a gated mode synchronously with the Nd:YAG laser. The ASE signal was detected through a pinhole 0.05 cm in diameter placed at a distance of ca. 50 cm from the sample cell. To measure the gain coefficient values ($\alpha(\lambda)$),[28] an optically calibrated half-cell shutter was placed between the primary laser excitation beam and the cell in order to block one-half the intensity of the excitation beam. The intensities (I) of the primary laser excitation at the respective full-cell length (L= 0.8 cm) and half-cell length ($L/2$ = 0.4 cm) of the shutter were optically calibrated with a volume absorbing disk calorimeter (Scientech, Inc. model 36-0001).

$$\alpha(\lambda) = \frac{2}{L} \ln\left[\frac{I_L}{I_{L/2}} - 1\right] \quad (1)$$

The photostability of the molecules studied was demonstrated by monitoring the absorption spectra before and after the laser experiments using a cuvette 0.01 cm in optical length.

D. Materials. The 2-phenylimidazole molecule was purchased from Aldrich Chemical Co. and used as supplied. 2-(2′-Hydroxyphenyl)imidazole (2HOPI),[29] 1-methyl-2-phenylimidazole,[30] 2-(2′-methoxypheny)imidazole (2MeOPI), and 1-methyl-2-(2′-hydroxyphenyl)imidazole (1M2HOPI)[29] were synthesized as described elsewhere.[31] The NMR and X-ray analyses as well as the crystal and molecular structure were also published elsewhere.[31]

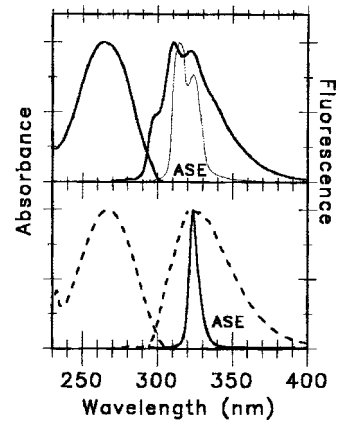

Figure 1. Absorption, fluorescence (λ_{exc} = 260 nm), and ASE spectra of 1-methyl-2-phenylimidazole in dioxane (bottom) and cyclohexane (top).

E. Theoretical Calculations. Ground-state (S_o) and first triplet-state (T_1) geometries were optimized using density functional theory[32,33] with the B3LYP hybrid functional and the 6-31G** basis set.[34] All calculations were executed by employing the GAUSSIAN 03 package[35] and the SPARTAN 4.1 program.[36] The global minima were checked by means of vibrational frequency analyses. All the structures thus identified were found to correspond to true minima as they had all real vibrational frequencies. Calculations on the first singlet excited state were executed at the time-dependent (TD) DFT level[37,38] and also with the CIS[39] methodology by utilizing the split-valence 6-31G** basis set. The proton-transfer potential-energy curves were calculated with full geometry optimization for the stationary points in the S_o and T_1 states and for the intermediate geometry points by fixing the OH distances and allowing the remaining coordinates to be optimized without constraints.

The S_1 state energy was estimated following two procedures: (i) with the aid of the S_o-optimized geometry at the DFT level and TD-DFT calculations [TD/DFT(S_o)] and (ii) the TD/CIS approach, which is based upon using (a) CIS methodology by keeping the hydrogen-bond coordinates of the fully optimized S_o structure at the DFT level fixed (i.e., N3—H2′, H2′—O2′, O2′—C2′, N3—H2′—O2′, Scheme 1) and allowing the remaining coordinates to be fully optimized and (b) subsequently the final geometry is obtained in a TD-DFT calculation. Use of only the CIS methodology *without constraints* provides very unreliable results for molecular systems with intramolecular hydrogen bonds.[21–23]

III. Results and Discussion

A. Absorption and Fluorescence Spectroscopy and ASE of 1-Methyl-2-phenylimidazole. The fluorescence spectroscopy and amplified spontaneous emission (ASE) of 2-phenylimidazole, 2-phenylbenzimidazole, and 1-methyl-2-phenylbenzimidazole in dioxane were reported previously.[12] They exhibit high ASE spikes at 320, 341, and 345.5 nm, respectively, with high laser gain values of ca. 10 cm^{-1}. Also, the 1-methyl-2-phenylimidazole molecule presents ASE at 323.5 nm in dioxane (Figure 1). In the current work, the N-methyl substitution emphasizes the inter-ring torsional—vibrational mechanism which explains how this molecule achieves population inversion.

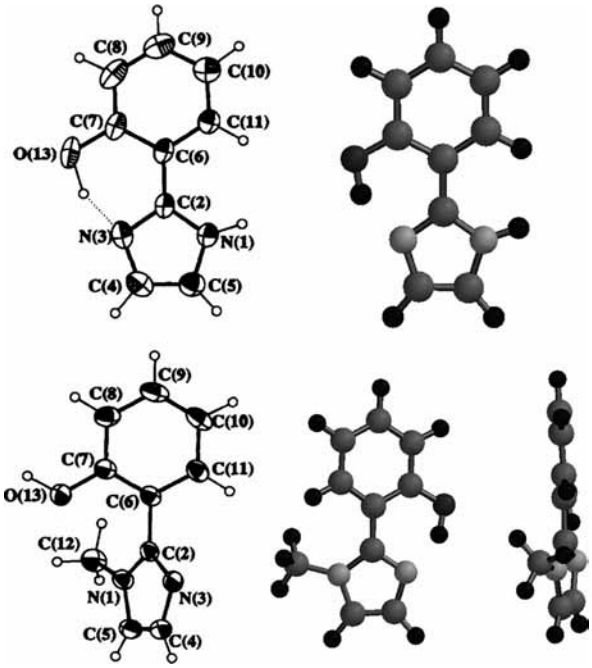

Figure 2. (Left) ORTEP view[24] of compounds 2-(2′-hydroxyphenyl)imidazole (2HOPI) and 1-methyl-2-(2′-hydroxyphenyl)imidazole (1M2HOPI). (Right) Calculated molecular structures of 2HOPI and 1M2HOPI at the DFT/B3LYP level for the ground electronic state; 1M2HOPI is presented in two views in order to emphasize the absence of coplanarity.

Indeed, in cyclohexane 2-phenylimidazole did not yield lasing action, also owing to low solubility; its concentration could not be larger than 4.3×10^{-3} M; however, the 1-methyl derivative at 4.2×10^{-3} M gives rise to dual-peak ASE at 314.5 and 323.5 nm (Figure 1), thus providing the shortest laser radiation reported up to date. The shortest tunable laser was technically reported[2,3,40] for 2,2′-dimethyl-*p*-terphenyl with a peak laser wavelength at 336 nm. The laser-gain spectrum for the 1-methyl-2-phenylimidazole is implemented in the Supporting Information (SI, Sfig-1) and shows a constant gain value of 5 cm^{-1} from 310 to 317 nm in cyclohexane and a gain value of ca. 8 cm^{-1} at 323.5nm in dioxane. The 1N-methylated molecules possess larger inter-ring dihedral angles in the ground electronic state than those for their analogues without methyl groups.[12] Indeed, upon photoexcitation they all tend to be coplanar, but the inter-ring dihedral angle changes to a greater extent for the methylated ones; for instance, for 2-phenylbenzimidazole it is 20° in the S_o state and changes to 0° in the S_1 state, but for its 1N-methylated derivative it changes from 42° (S_o) to 2° (S_1).[12]

The molecules 2HOPI and 1M2HOPI comprise one imidazole ring covalently linked to a phenol group, thereby implementing both feasible processes: ESIPT and inter-ring torsion. The coupling of both motions is investigated in the following sections.

B. Absorption and Fluorescence Spectroscopy in 2-(2′-Hydroxyphenyl)imidazoles. The molecular structures of some 2-(2′-hydroxyphenyl)imidazoles were determined by X-ray crystallography (Figure 2 and SI, Table S1).[31] The 2HOPI molecule contains a strong intramolecular hydrogen bond (IMHB) in crystal phase. The inter-ring torsional angle of −1.2° and the IMHB dihedral angle of −3.2° yield a quasi-planar molecular structure. This structure differs from that of the 1-methyl derivative, 1M2HOPI, which does not exhibit IMHB in the crystal phase (Figure 2); indeed, the hydroxyl-phenyl group is twisted and thus facing the 1-methyl group, forming the trans

SCHEME 2: Molecular Structures for 2HOPI [a]

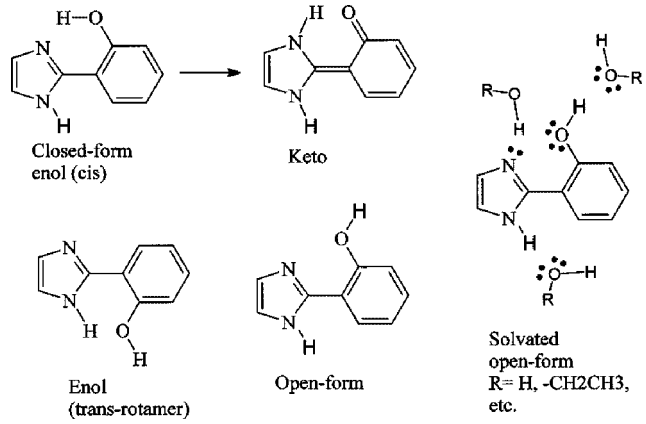

[a] The 1M2HOPI molecule possesses the same type of molecular structures; however, the enol trans rotamer proves to be another open form.

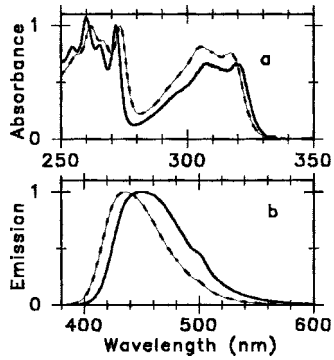

Figure 3. Absorption (top) and fluorescence (bpttom, $\lambda_{exc} = 320$ nm) spectra of 2HOPI in dioxane (dash line) and cyclohexane (solid line) at 298 K,

rotamer molecule (Scheme 2, another open form). The inter-ring dihedral angle for 1M2HOPI is −116.8° (+63.2°), and the hydroxy vs imidazole dihedral angle results in −153.2° (+26.8°). In the crystal phase 2HOPI and 1M2HOPI form chains through N−H···O and O−H···N intermolecular hydrogen bonds, respectively.

2-(2′-Hydroxyphenyl)imidazole (2HOPI). Absorption spectra for 2HOPI in cyclohexane and dioxane solutions at RT, Figure 3, exhibit vibronic structure. In cyclohexane the first absorption band shows peaks at 320.2 and 307.8 nm. In dioxane that absorption band is shifted to the blue and the vibronic structure is preserved. This blue shift may be due to lower polarity in the excited state than in the ground state or to greater distortion of the molecule from planarity in dioxane. It may be assumed that 2HOPI adopts the planar structure with intramolecular hydrogen bonds, closed form (Scheme 2), in agreement with the X-ray studies.[31] As confirmed by the theoretical calculations at the B3LYP-DFT level, the closed form proves to be 13.1 and 5.8 kcal/mol (SI, Table S7) more stable than the open form and the intramolecular hydrogen-bonded trans rotamer (another closed-form), respectively. Upon photoexcitation of 2HOPI in cyclohexane and dioxane at RT the fluorescence spectra (Figure 3) show one emission band with wavelength maxima located at 450 and 435 nm, respectively. The wavelength shift between absorption and emission corresponds to 9000 cm^{-1}, a typical shift for an excited-state proton-transfer process consistent with predictions of the theoretical calculations (vide infra). The fluorescence−excitation spectrum resembles the corresponding absorption spectra (SI, Sfig-2). Therefore, the ground-state

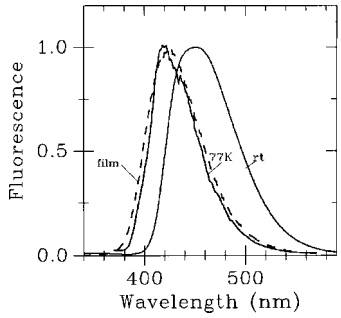

Figure 4. Fluorescence spectra (λ_{exc} = 300 nm) for 2HOPI in methylcyclohexane at RT (solid line) and 77 K (solid line) and in solid phase as a film in a quartz surface at RT (dashed line).

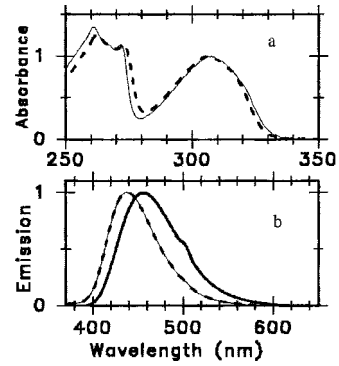

Figure 5. Absorption (top) and fluorescence (bottom, λ_{exc} = 320 nm) spectra of 1M2HOPI in dioxane (dash line) and cyclohexane (solid line) at 298 K.

molecular source of this emission is the closed form (enol cis, Scheme 2), the intramolecularly hydrogen-bonded 2HOPI species. The proton-transfer fluorescence quantum yield measured in cyclohexane is 0.51 with a lifetime of 4.2 ns. From these data, a radiative rate (k_f) of 1.2×10^8 s^{-1} is calculated. On the assumption that the proton-transfer tautomer forms with unit quantum yield in the first singlet excited state.

A peculiarity of this molecule shows up at 77 K. The emission spectrum in methylcyclohexane is blue shifted to 420 nm (Figure 4). The corresponding excitation spectrum at 77 K is also blue shifted, but not much, with respect to the RT absorption, thus peaking at 319 nm for the first band (SI, Sfig-3). Yet the wavenumber shift between the emission spectrum and its excitation spectrum at 77 K is ca. 7500 cm^{-1}, which still indicates a proton-transfer process in the excited state. Methylcyclohexane gives clear solutions down to −126.6 °C (melting point, mp), and below this temperature it forms clear glass matrices, which are adequate for spectroscopic studies.

Viscosity was checked at RT using squalane ($C_{30}H_{62}$) as solvent. Squalane exhibits a large viscosity even at 25 °C (28 cp)[41] in comparison with that of cyclohexane (0.89 cp) or methylcyclohexane (0.68 cp). Neither the absorption nor the emission spectra of 2HOPI in squalane exhibits differences with respect to the spectra in cyclohexane or methylcyclohexane. For instance, they show the same wavelength peak position and half-width as well as approximately the same vibronic structure. Yet it is not a definitive experiment; methylcyclohexane at 77.5 K possesses an estimated viscosity of 10^{17} P.[42]

To determine whether the change in temperature is responsible for the blue shift, a cell of 1 cm path length was seeded with 2HOPI powder. The cell was sealed and heated to ca. 70 °C. At this temperature the sample partially undergoes sublimation from the solid to the gas phase inside the cell. The cell was then placed into a thermostat at 25 °C. This sudden decrease of temperature deposits the sample like a thin film of microcrystals on the walls of the cell. Thereafter, an absorption spectrum was recorded (SI, Sfig-3), which resembles that obtained in methylcyclohexane at RT. The fluorescence emission for this film at RT matches (Figure 4) that emission band recorded for a methylcyclohexane solution at 77 K. Therefore, the temperature is not the crucial parameter for the wavelength shift observed from 450 to 420 nm (1587 cm^{-1}). The possibility of aggregation at lower temperatures than RT will be tested in 2-methylbutane (vide infra).

The above-mentioned experiments were made in the absence of solvent; therefore, viscosity is not a crucial parameter to observe the same emission blue shift.

1-Methyl-2-(2′-hydroxyphenyl)imidazole (1M2HOPI). For 1M2HOPI, the X-ray information reveals that the trans rotamer (Figure 2, an open form) is the most stable structure in the solid state.[31] However, these results do not correlate with the experimental evidence in solution at RT. Figure 5 shows that the absorption spectra of 1M2HOPI in cyclohexane and *p*-dioxane resemble each other. Compared with those of the 2HOPI molecule (Figure 3), the additional 1N methyl group causes no significant energy shift to the blue. If 1M2HOPI did not possess any intramolecular hydrogen bond, its absorption spectrum would have been significantly blue shifted compared with that of 2HOPI. Therefore, it is evident that 1M2HOPI possesses an intramolecular hydrogen bond in cyclohexane, dioxane, and even dimethyl sulfoxide (SI, cf. SFig-9). The absorption onset for 1M2HOPI is slightly red shifted as compared with that of 2HOPI owing to a small inductive effect from the methyl group. However, because the first absorption band of the 1M2HOPI molecule, with only one maximum at 307.6 nm in cyclohexane, shows no vibronic structure, coplanarity of the phenyl and imidazole rings is probably absent in the ground state. Nonplanar structures at variable torsional angle exhibit smaller absorption coefficients than coplanar ones and blend to blur the vibronic structure for the first absorption band.[43]

Upon photoexcitation, 1M2HOPI in cyclohexane emits fluorescence at ca. 462 nm (Figure 5) with a quantum yield of 0.23 and a lifetime of 2.2 ns. This gives a radiative rate constant of 1.1×10^8 s^{-1}, which equals that obtained for 2HOPI, on the assumption that the proton-transfer tautomer forms with unit quantum yield. The wavelength shift between the absorption and emission proves to be ca. 10 800 cm^{-1}, and therefore, it can be ascribed to the keto species formed upon ESIPT. The fluorescence−excitation spectrum resembles the absorption spectrum at RT.

As the temperature is decreased down to 77 K, on quick freezing in anhydrous (stored over sodium wire) cyclohexane solution, the fluorescence emission shifts to the blue, approximately going from 462 nm at RT to 428 nm at 77 K (1719 cm^{-1}) (Sfig-4). In dry cyclohexane at 77 K only the proton-transfer emission at 428 nm is present on excitation at 290 nm.

However, for 1M2HOPI in cyclohexane (not stored over sodium wire) at 77 K in addition to a long-wavelength emission at 434 nm another emission appears at ca. 326 nm (SI, Sfig-4). The latter emission exhibits a fluorescence−excitation spectrum by monitoring light emission at 330 nm with a maximum at 284 nm and onset at 305 nm, which is blue shifted in comparison with the absorption spectrum at RT. Therefore, its ground-state molecular source comes from the open-form species of 1M2HOPI. It is possible that these open-form species are also present at RT but in a minor contribution, and therefore, its emission could not be easily observed. As can be demonstrated, on excitation

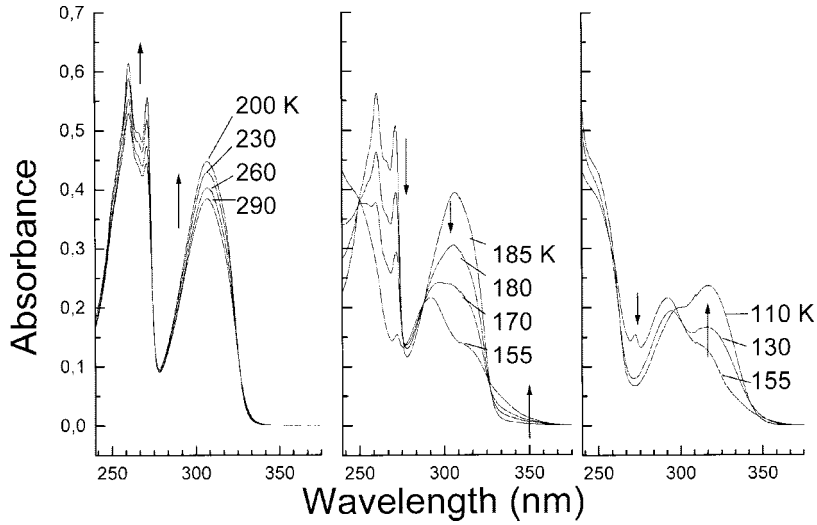

Figure 6. Low-temperature absorption spectra for 1M2HOPI, obtained at slow freezing from 290 to 110 K, in 2-methylbutane.

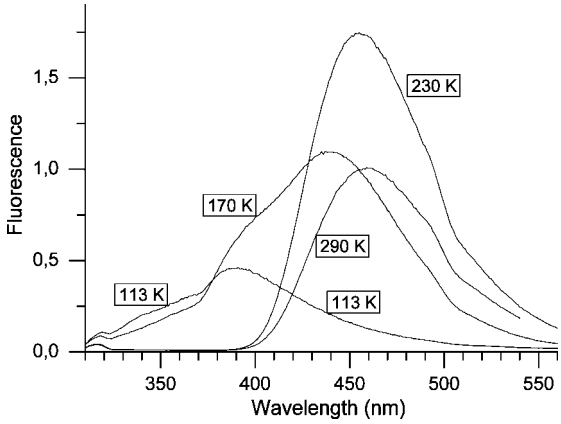

Figure 7. Emission spectra for 1M2HOPI in 2-methylbutane from 290 to 113 K, which are recorded using slow freezing. All spectra were recorded on excitation at 290 nm.

at 270 nm in cyclohexane at RT, a fluorescence band appears at ca. 326 nm which resembles that obtained at 77 K. Therefore, the absorption spectra for 1M2HOPI in cyclohexane (not stored over sodium wire) are multicomponent, thus consisting at least of one open-form species and the IMHB species (closed form) in chemical equilibrium (Scheme 2). The open-form species could be one of two types: the open form in Scheme 2 or the trans rotamer in Scheme 1 (another open form for 1M2HOPI). The main fluorescence band in cyclohexane at RT always corresponds to the proton-transfer tautomer emission; at 77 K in cyclohexane (not stored over sodium wire), however, the open-form emission dominates (SI, Sfig-4). On the other hand, by monitoring light at 420 nm it shows an excitation spectrum with peaks at 324 and 343 nm and with onset at ca. 370 nm, which is red shifted with respect to the absorption spectrum recorded at RT, and it could be ascribed to aggregate formation (vide infra, cf. Figures 6 and 7). Therefore, the emission band at 434 nm could be composed of both the keto tautomer and aggregate emission. Tiny water content plays an important role, since for the anhydrous cyclohexane 1M2HOPI shows neither the open-form emission nor the aggregate emission.

However, not only for 1M2HOPI in cyclohexane, dioxane, and dimethyl sulfoxide (DMSO, SI, Sfig-5) but also for 2HOPI in all the solvents the open-form emission at short wavelengths is present, though in a minor contribution (Sfig-6, S1). The NMR spectrum[31] indicates that the most stable structure in the ground electronic state corresponds to the IMHB structure, closed form (Scheme 2) for 2HOPI and 1M2HOPI in $CDCl_3$. However, in DMSO, a mixture of closed form and open form is feasible, thus indicating that the OH•••N intramolecular hydrogen bonds are partially broken. This could be due to the interaction of these molecules with traces of water (cf. Sfig-4). The main reason lies in the intrinsic effects of imidazoles, the affinity of the nitrogenous lone pairs for water, based on the large basicity of the nitrogen and large solvent acidity of water. Imidazole exhibits a larger basicity than pyridine; for instance, imidazole shows a proton affinity (PA) of 223.6 kcal/mol[44] in the gas phase vs that of 220.8 kcal/mol[45] for pyridine and a pK_b of 7.11[44] in aqueous solution compared to 5.35[45] for pyridine. On the other hand, opposite of what is expected even in anhydrous cyclohexane, 2HOPI and 1M2HOPI may exhibit a very tiny emission band at about 326 nm, unobservable unless one looks at it purposely by increasing the voltage of the photodetector. It is right to state that the large basicity of the pyridinic nitrogen may favor the intermolecular hydrogen-bond interaction as concluded from X-ray data values.[31]

Low-Temperature Spectroscopy for 1M2HOPI in 2-Methylbutane. We have chosen the solvent 2-methylbutane (mp at −159.9 °C, 113.25 K) because it exhibits clearer solutions below 126 K than methylcyclohexane and also below 110 K it shows a clear glass matrix, which is adequate for fluorescence and absorption spectroscopic studies. To evaluate possible aggregation effects we recorded absorption spectra as the temperature was decreased slowly in a cryostat. The experiments start with a dilute solution at RT in which only monomer is present. Subsequently, as the temperature is lowered aggregation effects may be recorded in accordance with an exothermic reaction. As shown in Figure 6, from 290 to 200 K the profile exhibits minor changes; it shows an increase in the relative absorbance within the wavelength range. This set of spectra corresponds mostly to the monomer species assigned to the IMHB closed form. From 185 to 155 K, the absorption spectra exhibit isosbestic points which are well defined for the spectra at 185, 180, and 170 K. The closed-form absorption band with a maximum at 307 nm is being suppressed, and the first absorption band splits into two bands, one shifted to the red and another to the blue, which is a well-known characteristic of aggregation.[46] The spectral characteristics of the closed-form monomer appears, though to a minor extent, even at 155 K (i.e., a peak absorption at ca. 272 nm is monitored). Therefore, monomer

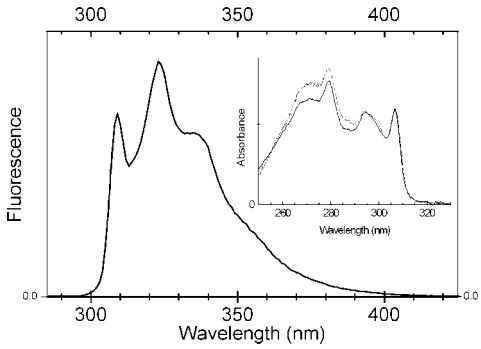

Figure 8. Absorption and fluorescence−excitation spectra (inset, λ_{em} = 350 nm) and fluorescence spectrum (λ_{exc} = 270 nm) of 2MeOPI in cyclohexane at 298 K.

and aggregate are present in chemical equilibrium. At 130 and 110 K the closed form monomer seems to have disappeared as the spectra differ significantly from that at 290 K. In addition, they show another isosbestic point that differs from the one which appears from 155 to 185 K. Therefore, it is concluded that a different aggregation process has taken placed, the first absorption band shifting to the red of that found at 155 K.

The fluorescence spectra were recorded also from 290 to 113 K with the same technique as above using a slow-freezing technique described in the Theoretical and Experimental Methods section. Figure 7 shows four emission spectra at 290, 230, 170, and 113 K on excitation at 290 nm. The fluorescence bands at 290 and 230 K are centered at 460.5 and 454.5 nm, respectively, thus showing a blue shift as the temperature decreases. In contrast, at 170 and 113 K the spectrum changes and shifts to the blue, thus showing, in accordance to the excitation spectra (not shown), a complex band of at least three components.

The absorption and emission spectra agree well with that below 155 K: the IMHB closed-form species disappears by generating new aggregates.

Also, below 200 K the excitation spectra by monitoring at 365 nm are characterized by a wavelength maximum at ca. 290−300 nm and an onset at a shorter wavelength than that for the closed-form monomer, which can be assigned to the open-form species. On excitation at 350 nm the emission spectra yields an emission band with a peak maximum at 460.5 nm for 290 K, at 454.5 nm for 230 K, at 408 nm for 170 K, and at 424 nm for 113 K. Spectra for the highest two temperatures reveal an emission band from the closed-form monomer species, whereas spectra for the lowest two temperatures exhibit emission bands that can be assigned to aggregates and open forms.

The emission spectrum at 113 K in Figure 7 differs greatly from those at 77 K in cyclohexane (SI, SFig-4). This difference is based on the quality of the matrices formed in cyclohexane and 2-methylbutane and how they have been frozen. The 2-methylbutane solvent forms a clear matrix at 113 K by slow freezing; however, cyclohexane (mp at 4−5 C) does not form a clear matrix at 77 K because of cracking and formation of a white solid. Conversely to cyclohexane at 77 K (SI, SFig-4), in which IMHB closed-form species of 1M2HOPI get trapped by quick freezing as well as the open-form species, the 2-methylbutane matrix by slow freezing at 113 K does not trap IMHB closed-form species (Figure 7).

2-(2′-Methoxypheny)imidazole (2MeOPI). For the sake of comparison, the spectroscopy of the 2-methoxy derivative of 2HOPI was studied. The absorption spectrum in cyclohexane for 2MeOPI at RT is blue shifted compared to those of 2HOPI and 1M2HOPI (Figure 8). This shows that the ground-state structure corresponds to open-form species. The absorption spectrum for the closed species would have appeared at about the same wavelength position as that for 2HOPI and 1M2HOPI. Nevertheless, the 2MeOPI absorption spectrum ends up in a tail at much longer wavelengths than that of the first absorption peak. In cyclohexane, the fluorescence spectrum of 2MeOPI exhibits seemingly a single band at ca. 336 nm (Figure 8). However, the fluorescence−excitation spectrum at 370 nm resembles the absorption spectrum, while the excitation spectra by monitoring fluorescence at 400 nm resemble the closed-form species of 2HOPI or 1M2HOPI in cyclohexane (Sfig-7, SI). One must conclude that the fluorescence spectrum is multicomponent as well as the absorption one, and therefore, the long-wavelength tail observed in the absorption spectrum corresponds to a minor contribution of the 2MeOPI closed form, which is in chemical equilibrium with the open form. This indicates that the intramolecular hydrogen bond in 2MeOPI is much less stronger than for its 4,5-dimethyl derivative,[18] which shows an absorption spectrum assigned only to the closed form. Certainly, the 4,5-dimethyl substitutions provide a stronger IMHB owing to inductive effects, which increase the basicity of the nitrogen N3.

In dioxane and dimethyl sulfoxide (DMSO), the 2MeOPI closed-form excitation spectrum was not found on monitoring at the long-wavelength tail of the fluorescence band. In these solvents, only the open-form species is present (Sfig-8, SI). On photoexcitation at 270 nm in cyclohexane and at 300 nm in dioxane and DMSO 2MeOPI presents fluorescence quantum yields of 0.29 for the first two solvents and 0.21 for the last one.

The theoretical calculations (SI, Table S1−S6) for the molecular conformers of 2HOPI and 1M2HOPI were performed at the B3LYP (DFT) level, and all of them exhibit real vibrational frequencies. Actually, the structures trans rotamer and open form of 2HOPI in Table S7 (SI) may be ascribed to those structures for 2MeOPI. The free energies obtained for the isolated conformers (SI, Table S7) indicate that the closed form (cis-enol form) is the most stable, thus corresponding to the hydrocarbon−solvent observations reported above for 2HOPI and 1M2HOPI at RT. However, in solution the open forms are also monitored for emission and absorption, which does not correspond to the calculations for the isolated molecules. The calculations predict that the 2HOPI trans rotamer (also a closed-form, with a weak intramolecular hydrogen bond) possesses a smaller free energy than that for the corresponding open form (SI, Table S7). However, solvent effects were not implemented in the calculations for the sake of simplicity.

The absorption and emission data for 2MeOPI measured (SFig-9 and SFig-10) in hydrocarbon, dioxane, methanol, DMSO, and water point to solvent acidity as the main reason for the predominant generation of the open form in the ground state (Scheme 2, solvated open form). It is in methanol and water solutions rather than in DMSO and 1,4-dioxane that the open-form species is generated to a greater extent as monitored for both absorption and emission measurements. In accordance with the pure solvent scales (SPP, SB, and SA),[47] water exhibits a negligible solvent basicity (SB, 0.025), large solvent acidity (SA, 1.062), and large dipolarity/polarizability (SPP, 0.962). This behavior makes a good contrast with DMSO; this solvent presents a negligible SA (0.072) value and large SPP (1.000) and SB (0.647). The solvent 1,4-dioxane exhibits 0 for SA, 0.701 for SPP, and 0.444 for SB. Furthermore, DMSO and dioxane may contain water to some extent, which interacts with the

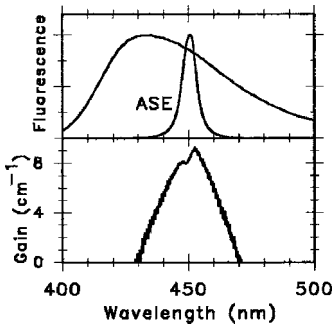

Figure 9. Fluorescence (at low concentration, λ_{exc}=306 nm) and ASE (at high concentration, λ_{exc}=266 nm) spectra in dioxane for 2HOPI (top). Correspondingly, the gain spectrum in cm^{-1} (cf. Theoretical and Experimental Methods section) is shown in the bottom graphic.

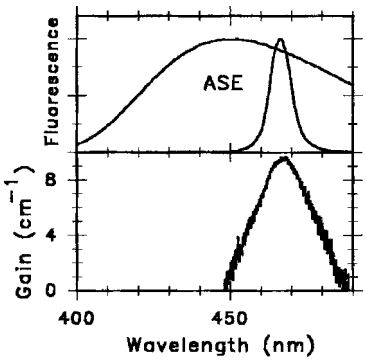

Figure 10. Fluorescence (at low concentration, λ_{exc} = 270 nm) and ASE (at high concentration, λ_{exc} = 266 nm) spectra in dioxane for 1M2HOPI. Correspondingly, the gain spectrum in cm^{-1} (cf. Theoretical and Experimental Methods section) is shown in the bottom graphic.

2MeOPI molecule, thereby generating solvated open-form structures and shifting to the blue its fluorescence and absorption spectra.

C. Amplified Spontaneous Emission (ASE) in 2-(2′-Hydroxyphenyl)imidazoles. A good amplified spontaneous emission for 2HOPI (Figure 9) and 1M2HOPI (Figure 10) was obtained in dioxane at 298 K rather than in cyclohexane, owing to their limited solubility in cyclohexane. Both molecular systems show that the ASE spike (at 450 nm for 2HOPI and 466 nm for 1M2HOPI) comes from the proton-transfer tautomer at about 15 nm to the red of the wavelength maximum of the respective fluorescence spectrum of a dilute solution. This red shift is also observed for the single-crystal sample of acetic acid 2-{4-[2-(2-hydroxyphenyl)-4,5-diphenylimidazol-1-yl]phenyl}-ethylester (**15**, structure in SI) comparing the ASE at 3.5 mJ cm^{-2} pulse^{-1} with the corresponding emission at low laser excitation of 0.11 mJ cm^{-2} pulse^{-1}. This red shift could be due to excited-state transient absorption. Indeed, excited-state transient absorption has been reported as the main reason for suppressing the lasing action in 2-phenyloxazole, stilbene, and other molecules.[28] In addition, the fluorescence emission from all-*trans*-1,6-diphenyl-1,3,5-hexatriene upon increasing the laser excitation energy shifts to the red owing to excited-state transient absorption.[48] An alternative explanation was reported for the polyhydroxyflavones;[49] the red shift was attributed to a dipolar field effect caused by the large concentrations employed in the ASE experiments.

The gain spectra (Figures 9 and 10) show high peak values centered at 452.6 and 468 nm of 9.3 and 9.5 cm^{-1} for 2HOPI and 1M2HOPI in dioxane, respectively. A low gain value of 1.5 cm^{-1} at the maximum of the emission band was obtained for 2HOPI (3.9×10^{-3} M) in cyclohexane solution; under the same conditions, 1M2HOPI does not exhibit lasing action, not even bubbling argon gas to avoid secondary reactions with oxygen.

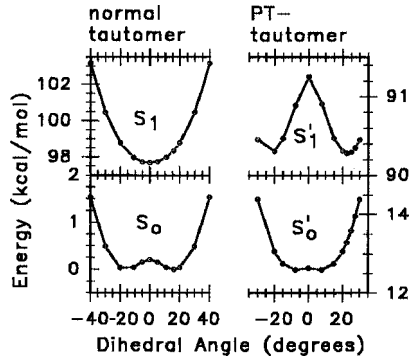

Figure 11. Energy diagram of 1M2HOPI vs the dihedral inter-ring angle (N3C2N1′C2′, cf. Scheme 1) for both tautomers, enol (normal tautomer) and keto (proton-transfer tautomer), in the ground electronic state (bottom, calculated at the DFT level) and in the first singlet excited electronic state (top, at the TD/DFT level).

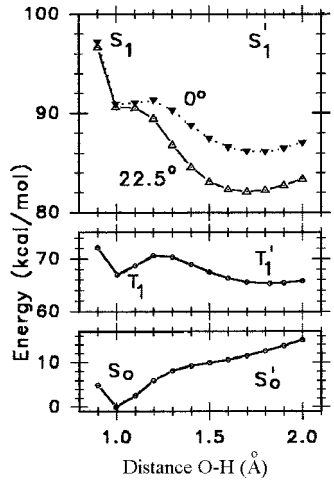

Figure 12. Potential-energy curves for the proton-transfer process of 1M2HOPI in the ground electronic state (at DFT level), first triplet state (at DFT level), and first singlet excited state (at TD/CIS/DFT level) vs the OH stretching coordinate in Angstroms (Å). S_1 and T_1 refer to the normal tautomer, and S_1' and T_1' refer to the proton-transfer tautomer. The dihedral angles 22.5° and 0° were fixed for the corresponding curves in the first singlet excited state.

IV. Theoretical Calculations and Laser Mechanism in 2-(2′-Hydroxyphenyl)imidazoles

The theoretical calculations at the DFT level for the ground state predict a nonplanar structure for 1M2HOPI with inter-ring dihedral angles of 19° and −19° separated by a small barrier of ca. 0.2 kcal/mol in energy (Figure 11). Upon photoexcitation, however, the molecular structure in S_1 becomes coplanar. The global energy minimum for S_1 corresponds to a structure with an inter-ring dihedral angle of 0°. From this structure in the singlet manifold the subsequent proton-transfer process has been investigated. A coupling of the torsional vibrational motion with the proton-transfer reaction gives rise to an intricate and unexpected behavior. The proton-transfer tautomer in the ground state does not present a minimum (Figure 12) but a repulsive potential-energy curve. In the S_1 state, however, the most stable tautomer (proton-transfer tautomer) is nonplanar with inter-ring torsional angles of about 22.5° or −22.5°, the two structures separated by a barrier of 2 kcal/mol. Therefore, upon photoex-

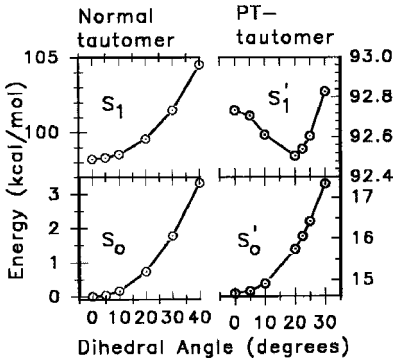

Figure 13. Energy diagram of 2HOPI vs the dihedral inter-ring angle (N3C2N1′C2′, cf. Scheme 1) for both tautomers, enol (normal tautomer) and keto (proton-transfer tautomer), in the ground electronic state (bottom, calculated at the DFT level) and in the first singlet excited electronic state (top, at the TD/DFT level).

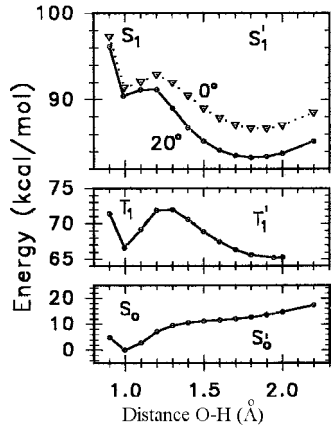

Figure 14. Potential-energy curves for the proton-transfer process of 2HOPI in the ground electronic state (at DFT level), first triplet state (at DFT level), and first singlet excited state (at TD/CIS/DFT level) vs the OH stretching coordinate in Angstroms (Å). S_1 and T_1 refer to the normal tautomer, and S_1' and T_1' refer to the proton-transfer tautomer. The dihedral angle was fixed on 22.5° and 0° in order to obtain the curves in the S_1-S_1' state.

citation of the normal tautomer the 1M2HOPI molecule becomes coplanar and undergoes an exothermic proton transfer in the S_1 state, which corresponds to a nonplanar conformation.

In contrast to the S_o state, the calculations predict an exothermic proton-transfer process over a small barrier in the lowest triplet state (Figure 12). The T_1 proton-transfer process is dictated by the change from a nonplanar structure (5.0°), normal tautomer, to another nonplanar structure (6.4°), the proton-transfer tautomer. An important feature of this proton-transfer process relies on how the proton is transferred from oxygen to nitrogen; the inter-ring torsion precedes the proton transfer. By plotting the inter-ring dihedral angle vs the OH distance (Sfig-11) it is observed that though the two tautomer minima possess nonplanar conformations, the proton is transferred from the coplanar conformation with a dihedral angle of 0° for the OH distances from 1.1 to 1.7 Å.

The same prototype behavior is found for the 2HOPI molecule. The normal tautomer is found to be more planar in S_o than in S_1 (Figure 13). For a Boltzmann distribution at energy RT ($RT = 0.59$ kcal/mol; $R = 1.995$ kcal/mol, $T = 298.15$ K) the molecular structure possesses a more nonplanar structure in S_o than in S_1. However, the proton-transfer tautomer of 2HOPI does not possess a coplanar structure (Figures 13 and 14) as well as that of the 1M2HOPI molecule. The most stable proton-transfer structure exhibits an inter-ring dihedral angle at about 20° in the first singlet state. The inter-ring torsional motion produces an extra stabilization of the proton-transfer tautomer, thus producing a large inter-ring dihedral angle, though it maintains an intramolecular hydrogen bond. The inter-ring torsion modulates the ESIPT process, and both motions are necessary to explain the fluorescence spectroscopy of the 2-(2′-hydroxyphenyl)imidazole molecules.

In the T_1 state, the 2HOPI normal tautomer with the 1H atom in the imidazole plane develops an imaginary frequency unless this hydrogen atom becomes pyramidalized. However, the proton-transfer tautomer exhibits the 1H atom in the imidazole plane in accordance with a longer inter-ring length of 1.40 vs 1.37 Å for the normal tautomer. The first triplet state undergoes an exothermic proton-transfer reaction (Figure 14) over a small barrier, thus showing two nonplanar tautomers, with coplanar structures at intermediate hydroxyl stretching coordinates. As in the case of 1M2HOPI, the inter-ring torsion precedes proton transfer.

A. Population-Inversion Mechanism. If for 3-hydroxyflavone[50] and other intramolecular hydrogen-bonded systems the OH stretching along the proton-transfer process in S_1 proves to be the predominant mechanism for population inversion and hence ASE spike appearance and for 1-methyl-2-phenylimidazole the inter-ring torsional vibration is responsible for the laser population inversion,[12] it is clear that for the 2-(2′-hydroxyphenyl)imidazoles a complex model made of both motions can be effective (Figures 11 and 14). Coupled to each other, the inter-ring torsional motion and OH stretching along the proton-transfer process in the excited state (cf. Figures 12 and 14) provide the population inversion necessary for ASE to show up under the right parameters of concentration, laser excitation, and adequate solvent, which allow 2HOPI and 1M2HOPI to overcome their respective laser thresholds.

The main contribution to the total energy for the ESIPT process comes from the OH stretching, and the inter-ring torsional motion modulates the OH total energy by lowering it in ca. 3.4 kcal/mol (cf. Figures 12 and 14) on going from an inter-ring dihedral angle of ca. 0° for the normal tautomer to about 20−22.5° for the proton-transfer tautomer.

B. Coupling between the Motions OH Stretching and Inter-Ring Torsion. Preliminary calculations for 2HOPI at the TD/DFT level with full geometry optimization in the first singlet excited state predict a minimum for the enol tautomer (closed form). The S_1 enol structure is coplanar (inter-ring dihedral angle, N3C2C1′C2′ = 0.05°) as well as the enol structure in the ground electronic state. We present those vibrational frequency normal modes (low-frequency modes) for the first singlet excited state of the 2HOPI enol form, which exhibit skeletal motions (i.e., inter-ring torsion), and OH stretching coupled to one another, which may prove the existence of the coupling between the inter-ring torsion and OH stretching along the ESIPT process. These modes should have an important component corresponding to the internal motion of the intramolecular O−H···O fragment and the inter-ring torsion acting simultaneously. Our analysis reveals at least the existence of three vibrational modes that couple the phenylimidazole inter-ring torsion with the motion of the O−H···O fragment, i.e., those vibrational modes corresponding to 130.2, 179.0, and 276.4 cm^{-1}. In addition, the large vibrational modes corresponding to 1669.9, 1613.9 (especially this one), 1540.2, 1525.3, and 1474.9 cm^{-1} involve skeletal motions and O−H stretching.

Another important feature from the vibrational analysis of the enol form lies in the change of the OH stretching frequency

on photoexcitation, that is, from 3226.8 cm^{-1} in the S_o state (at DFT level) to 2170.3 cm^{-1} in the S_1 state (at the TD/DFT level with full geometry optimization).

C. Photophysical Model for the 2HOPI, 1M2HOPI, and 2MeOPI Molecules. Discrepancies between the theoretical calculations and the experimental results are summarized in the following points.

(i) In hydrocarbon solution, the closed form is predicted to be the most stable species for both 2HOPI and 1M2HOPI (SI, Table S7) (ΔG open → closed = −5.8 and −13.1 kcal/mol, respectively). However, even in anhydrous cyclohexane a tiny emission at 326 nm is observed on excitation at 270 nm. Also, for 1M2HOPI in the crystal phase the most stable form is the trans rotamer (another open form).

(ii) The open form of the methoxy derivative 2MeOPI in cyclohexane is more stable than the closed form. The methoxy structure is analogous to the open form and trans rotamer of 2HOPI. In disagreement with the experimental evidence, the theoretical calculations (SI, Table S7) predict that the corresponding trans rotamer is more stable (open → trans rotamer; $\Delta G = -7.3$ kcal/mol) than the open-form structure.

(iii) Theoretical calculations (see Figures 12 and 14), which are appropriate for the gas phase, predict that upon ESIPT the most stable keto tautomer will have a large inter-ring dihedral angle. If so, the keto tautomer emits from a nonplanar structure. In contrast, as the solvent acidity increases the proton-transfer emission shifts to the blue, from 450 (hydrocarbon) to 410 nm (in water). Nevertheless, differing from the theoretical prediction, this solvent behavior is expected for a coplanar structure in cyclohexane, which departs from coplanarity as the solvent acidity increases, owing to solute−solvent intermolecular hydrogen bonding.

(iv) The 2HOPI and 1M2HOPI proton-transfer emissions that are centered at 450 and 462 nm at 298 K in hydrocarbon solution shift to 420 and 428 nm at 77 K, respectively. Neither the viscosity nor the temperature changes these shifts. Indeed, the emission spectra for a film of 2HOPI at RT peaks at 420 nm and resemble those found for 2HOPI in methylcyclohexane at 77 K.

(v) For 1M2HOPI in cyclohexane with some water content at 77 K, a dual emission is found, and the emission intensity for the open form at ca. 326 nm is greater than that of the proton-transfer/aggregate emission centered at ca. 434 nm. The presence of the open form at 77 K is inconsistent with the theoretical calculations, which predict that the open form and trans rotamer are 10.4 and 8.4 kcal/mol higher in energy than the closed form, respectively (Table S7, SI).

(vi) The first absorption bands of 2HOPI and 1M2HOPI in dioxane, DMSO, or methanol show as much vibronic structure as in hydrocarbon solution and are shifted to the blue of the corresponding band in hydrocarbon solution. Conversely for 2MeOPI in the same solvents, the absorption spectra lose vibronic structure and are shifted to the red of that in hydrocarbon solution.

All these seeming discrepancies stemming from multicomponent effects, on one hand, on photoexcitation ESIPT are undergone (for the isolated molecule) from the normal tautomer, which presents a coplanar phenylimidazole structure, to proton-transfer tautomer, which presents a nonplanar structure of about 20° in dihedral angle. On the other hand, these compounds, 2HOPI, and 1M2HOPI, form chains through N−H···O and O−H···N intermolecular hydrogen bonds, respectively, in the solid state (crystal structure) (SI, Sfig-12).[31] These intermolecular interactions must be present in hydrocarbon or other solvents (at RT or 77 K) and in films of microcrystals supported by the silica (quartz) wall. These interactions weaken the intramolecular hydrogen bond of 2HOPI and 1M2HOPI, thus distorting the inter-ring phenylimidazole dihedral angle and causing blue shifts for the electronic transitions studied. In fact, it was reported[51] on the physical and chemical adsorption of methyl salicylate in the silica (quartz) walls: "the polarity of methyl salicylate molecules renders its chemisorption on silica possible".[51] Methyl salicylate as well as 2HOPI and 1M2HOPI possess an intramolecular hydrogen bond that may be perturbed. This intermolecular interaction may quench the fluorescence for the crystal phase, thus suppressing the ASE or lasing action, as reported for many molecular systems. In the solid state, phenyl substitution at the 1, 4, and 5 positions (Sfig-13 and -14)[15] has proved to eliminate the solute−solute interactions, that is, the intermolecular chains of the type N−H···O or O−H···N (Sfig-12) found for 2HOPI and 1M2HOPI[31] get suppressed.

Conclusions

Methyl substitution at the 1N position of 2-phenylimidazole provides the shortest wavelength for a liquid-state laser-dye reported to date, thus yielding ASE in cyclohexane with a peak wavelength at 314.5 nm and a constant laser gain value of 5 cm^{-1}.

The 2-(2′-hydroxyphenyl)imidazole molecules give rise to amplified spontaneous emission (ASE) with high gain values (9 cm^{-1}) at 450 and 466 nm. The population inversion responsible for laser action, in accordance with the theoretical and experimental results, is understood in terms of a vibronic coupling between the hydroxyl stretching and the phenyl/imidazole inter-ring torsional motions.

The proton-transfer spectroscopy of 2-(2′-hydroxyphenyl)imidazoles was studied in dioxane, cyclohexane, dimethyl sulfoxide, methanol, and water. Solvent acidity is the main parameter which fosters formation of the open-form species in the ground electronic state. Methyl substitution at the 1N position weakens the intramolecular hydrogen bond, thus favoring formation of the solvated open species in 2-hydroxyphenylimidazoles as the solvent acidity increases, thus forming solute−solvent hydrogen-bonded species in the ground electronic state. This decreases the potential capacity of the molecular system to undergo ASE because of ESIPT. In accordance with X-ray analysis, these molecules form associations through intermolecular hydrogen-bonded chains of the type N−H···O or O−H···N in the solid state as well as in solution, thus explaining (i) the changes in the absorption spectra observed on lowering the temperature below 200 K, which are assigned to aggregation, (ii) the appearance of open-form emission at ca. 326 nm either at RT or 77 K, (iii) the anomalous blue shift found for the proton-transfer emission on lowering the temperature from 298 to 77 K in hydrocarbon solution, and (iv) the anomalous blue shift of the proton-transfer emission as the solvent acidity increases at RT.

Acknowledgment. We are indebted to the DGICYT of Spain for financial support (Projects CTQ2005-03052 and CTQ2006-02586). The Centro de Computación Científica of Universidad Autónoma de Madrid (Spain) is acknowledged for providing the CPU time facilities. We are pleased to acknowledge Prof. M. Kasha for allowing one of us (J.C.V.) to use his laboratory facilities and Drs. L. van de Burgt and D. A. Gormin of the Chemistry Laser Laboratory at Florida State University for their valuable assistance in laser optics. Referees are kindly acknowledged for their questioning and goodwill.

Supporting Information Available: Experimental and theoretical information. This material is available free of charge via the Internet at http://pubs.acs.org.

References and Notes

(1) Drexhage, K. H. Structure and Properties of Laser Dyes. *Top. Appl. Phys.* **1973**, *1*. (Dye Lasers), 144.

(2) King, T. A. Comprehensive Series in Photochemistry & Photobiology. *Lasers and Current Optical Techniques in Biology*; Palumbo, G., Protesi, R., Eds.; Royal Society of Chemistry: Cambridge, UK, 2004; Vol. 4, p 3.

(3) King, T. A. Comprehensive Series in Photochemistry & Photobiology. *Lasers and Current Optical Techniques in Biology*; Palumbo, G., Protesi, R., Eds.; Royal Society of Chemistry: Cambridge, UK, 2004; Vol. 4, p 33.

(4) Okasabu, K.; Kawachi, T.; Oyama, H.; Hara, T.; Yamaguchi, N.; Ando, K. *Jpn. J. Appl. Phys., Part 1* **2000**, *39*, 70.

(5) Davis, C. C.; King, T. A. *Adv. Quantum Electron.* **1975**, *3*, 169.

(6) Esslinger, T.; Bloch, I.; Hansch, T. W. *Phys. Blaetter* **2000**, *56* (2), 47.

(7) Khan, A.; Kasha, M. *Proc. Natl. Acad. Sci. U.S.A.* **1983**, *80*, 1767.

(8) Chou, P. T.; McMorrow, D.; Aartsma, T. J.; Kasha, M. *J. Phys. Chem.* **1984**, *88*, 4596.

(9) Acuña, A. U.; Costela, A.; Muñoz, J. M. *J. Phys. Chem.* **1986**, *90*, 2807.

(10) Acuña, A. U.; Amat-Guerri, F.; Catalán, J.; Costela, A.; Figuera, J. M.; Muñoz, J. M. *Chem. Phys. Lett.* **1986**, *132*, 567.

(11) Costela, A.; Amat-Guerri, F.; Catalán, J.; Douhal, A.; Figuera, J. M.; Muñoz, J. M.; Acuña, U. A. *Opt. Commun.* **1987**, *64*, 457.

(12) Catalán, J.; de Paz, J. L. G.; del Valle, J. C.; Kasha, M. *J. Phys. Chem. A* **1997**, *101*, 5284.

(13) Catalan, J.; Mena, E.; Fabero, F.; Amat-Guerri, F. *J. Chem. Phys.* **1992**, *96*, 2005.

(14) Fluorene (10^{-3} M) in cyclohexane solution on excitation at 266 nm does not yield lasing action. Several more concentrations and solvents were tried with identical results.

(15) Park, S.; Kwon, O.-H.; Kim, S.; Park, S.; Choi, M.-G.; Cha, M.; Park, S. Y.; Jang, D.-J. *J. Am. Chem. Soc.* **2005**, *127*, 10070.

(16) Douhal, A.; Amat-Guerri, F.; Lillo, M. P.; Acuña, A. U. *J. Photochem. Photobiol. A: Chem.* **1994**, *78*, 127.

(17) Testa, A. C. *Chem. Phys. Lett.* **1991**, *50*, 243.

(18) Bräuer, M.; Mosquera, M.; Pérez-Lustres, J. L.; Rodríguez-Prieto, F. *J. Phys. Chem. A* **1998**, *102*, 10736.

(19) (a) Purkayastha, P.; Chattopadhyay, N. *J. Mol. Struct.* **2002**, *604*, 87. (b) *Int. J. Mol. Sci.* **2003**, *4*, 335.

(20) Fóres, M.; Duran, M.; Solà, M.; Adamowicz, L. *J. Phys. Chem. A* **1999**, *103*, 4413.

(21) Catalán, J.; de Paz, J. L. G. *J. Phys. Chem. A* **2001**, *105* (30), 7315.

(22) Sobolewski, A. L.; Domcke, W. The Reaction Path in Chemistry: Current Approaches and Perspectives. In *Understanding Chemical Reactivity*; Heidrich, D., Ed.; Kluwer: Dordrecht, The Netherlands, 1995; Vol. 16, p 257.

(23) Sobolewski, A. L.; Domcke, W. *Chem. Phys.* **1998**, *232*, 257.

(24) Meech, S. R.; Phillips, D. *J. Photochem.* **1983**, *23*, 193.

(25) Catalán, J.; del Valle, J. C. *J. Am. Chem. Soc.* **1993**, *115*, 4321.

(26) del Valle, J. C.; Kasha, M.; Catalán, J. *Chem. Phys. Lett.* **1996**, *263*, 154.

(27) del Valle, J. C.; Kasha, M.; Catalán, J. *J. Phys. Chem. A* **1997**, *101*, 3260.

(28) Shank, C. V. *Rev. Mod. Phys.* **1975**, *47* (3), 649.

(29) Rogers, G. A.; Bruice, T. C. *J. Am. Chem. Soc.* **1974**, *96*, 2463.

(30) Mahmood, A.; Liu, H.; Joes, J. G.; Edwards, J. O.; Sweigart, D. A. *Inorg. Chem.* **1988**, *27*, 2149.

(31) Foces-Foces, C.; Llamas-Saiz, A. L.; Claramunt, R. M.; Cabildo, P.; Elguero, J. *J. Mol. Struct.* **1998**, *440*, 193.

(32) Becke, A. D. *J. Chem. Phys.* **1993**, *98*, 5648.

(33) Lee, C.; Yang, W.; Parr, R. G. *Phys. Rev. B* **1988**, *37*, 785.

(34) Hariharan, P. C.; Pople, J. A. *Chem. Phys. Lett.* **1972**, *16*, 217.

(35) Frisch, M. J.; Trucks, G. W.; Schlegel, H. B.; Scuseria, G. E.; Robb M. A.; Cheeseman, J. R.; Montgomery, J. A., Jr.; Vreven, T.; Kudin, K. N.; Burant, J. C.; Millam, J. M.; Iyengar, S. S.; Tomasi, J.; Barone, V.; Mennucci, B.; Cossi, M.; Scalmani, G.; Rega, N.; Petersson G. A.; Nakatsuji, H.; Hada, M.; Ehara, M.; Toyota, K.; Fukuda, R.; Hasegawa, J.; Ishida, M.; Nakajima, T.; Honda, Y.; Kitao, O.; Nakai, H.; Klene, M.; Li, X.; Knox, J. E.; Hratchian, H. P.; Cross, J. B.; Adamo, C.; Jaramillo, J.; Gomperts, R.; Stratmann, R. E.; Yazyev, O.; Austin, A. J.; Cammi, R.; Pomelli, C.; Ochterski, J. W.; Ayala, P. Y.; Morokuma, K.; Voth, G. A.; Salvador, P.; Dannenberg, J. J.; Zakrzewski, V. G.; Dapprich, S.; Daniels, A. D.; Strain, M. C.; Farkas, O.; Malick, D. K.; Rabuck, A. D.; Raghavachari, K.; Foresman, J. B.; Ortiz, J. V.; Cui, Q.; Baboul, A. G.; Clifford, S.; Cioslowski, J.; Stefanov, B. B.; Liu, G.; Liashenko, A.; Piskorz, P.; Komaromi, I.; Martin, R. L.; Fox, D. J.; Keith, T.; Al-Laham, M. A.; Peng, C. Y.; Nanayakkara, A.; Challacombe, M.; Gill, P. M.W.; Johnson, B.; Chen, W.; Wong, M. W.; Gonzalez, C.; Pople, J. A. *Gaussian 03*, Revision C.02; Gaussian, Inc.: Wallingford, CT, 2004.

(36) *SPARTAN*, Version 4.1; Wavefunction, Inc.: Irvine, CA, 1996.

(37) Hehre, W. J.; Radom, L.; Schleyer, R. V.; Pople, J. A. *Ab Initio Molecular Orbital Theory*; Wiley: New York, 1986.

(38) Casida, M. E. In *Recent Advances in Density Functional Methods, Part I*; Chang, D. P., Ed.; World Scientific: Singapore, 1995; Vol. 155.

(39) Foresman, J. B.; Head-Gordon, M.; Pople, J. A. *J. Phys. Chem.* **1992**, *96*, 135.

(40) Brackmann, U., Ed.; Lambdachrome Laser Dye; Lambda Physik GmbH: Göttingen, Germany, 1986.

(41) De Smet, K. *Phys. Rev. E* **1998**, *57*, 1384.

(42) Campbell, A.; Willard, J. E. *J. Phys. Chem. A* **1968**, *72*, 1918.

(43) Catalán, J. *Chem. Phys. Lett.* **2006**, *421*, 134.

(44) Catalán, J.; Claramunt, R. M.; Elguero, J.; Laynez, J.; Menéndez, M.; Anvía, F.; Avían, J. H.; Taagepera, M.; Taft, R. W. *J. Am. Chem. Soc.* **1988**, *110*, 4105.

(45) Lias, S. G.; Liebman, J. F.; Levin, R. D. *J. Phys. Chem. Ref. Data* **1984**, *13* (3), 695.

(46) McRae, E. G.; Kasha, M. The Molecular Exciton Model. In *Physical Processes in Radiation Biology*; Augenstein, L., Rosenberg, B., Mason, S. F., Eds.; Academic Press: New York, 1964; pp 23−42.

(47) Catalán, J. In *Handbook of Solvents*; Wypych, G., Ed.; W. A. Publishing: New York, ChemTec Publishing: Toronto, 2001.

(48) del Valle, J. C.; Tarkalanov, N.; Saltiel, J. *J. Phys. Chem. B* **1999**, *103*, 9350.

(49) Gormin, D.; Sytnik, A.; Kasha, M. *J. Phys. Chem. A* **1997**, *101*, 672.

(50) Del Valle, J. C. *J. Chem. Phys.* **2006**, *124*, 1.

(51) Acuña, A. U.; Catalán, J.; Toribio, F. *J. Phys. Chem.* **1981**, *85*, 241.

JP7117604